Analytical Methods

PAPER

View Article Online
View Journal | View Issue

Cite this: *Anal. Methods*, 2014, **6**, 7935

Impedimetric graphene-based biosensor for the detection of *Escherichia coli* DNA†

Nurulasma Zainudin,[a] Ab. Rahim Mohd Hairul,[a] Mashitah Mohd Yusoff,[a] Ling Ling Tan[b] and Kwok Feng Chong*[a]

Received 4th August 2014
Accepted 7th August 2014

DOI: 10.1039/c4ay01836b

www.rsc.org/methods

A label-free impedimetric DNA biosensor based on graphene nanosheets has been developed for the detection of *Escherichia coli* O157:H7 strain GZ-021210. Probe DNA (pDNA) of *E. coli* was immobilized onto graphene nanosheets by the surface functionalization of graphene with 1-pyrenebutyric acid (PyBA) followed by carbodiimide linkage. The hybridization of complementary DNA (cDNA) of *E. coli* with the immobilized pDNA increased the electron transfer resistance of the graphene nanosheets, as observed by electrochemical impedance spectroscopy (EIS). The *E. coli* DNA biosensor displayed a wide range of linear response (1.0×10^{-10} M to 1.0×10^{-14} M), low detection limit (0.7×10^{-15} M), single-base mismatch selectivity, high robustness and good reproducibility. The current work demonstrates an important advancement in the development of a sensitive biosensor for *E. coli* detection.

Introduction

Escherichia coli, better known as *E. coli*, is a dangerous pathogen that can cause stomach cramps, anaemia, haemorrhagic diarrhoea and kidney failure.[1–3] The contamination of food products with *E. coli* is a chronic worldwide problem that causes million dollar losses and presents a deadly threat to healthy living. The largest *E. coli* outbreak in 2011 infected more than 3950 people and caused 53 fatalities in Europe.[4] Therefore, it is essential to develop a specific monitoring system for *E. coli* in food products.

Conventional methods for *E. coli* detection include colony counting and immunoassay. These methods, however, have certain drawbacks such as being time consuming and requiring skilled laboratory personnel. Various methods have been proposed to improve the detection of *E. coli*, including optical,[5,6] calorimetric[7,8] and electrochemical methods.[9,10] Among these, electrochemical methods are proven to be an effective approach for rapid *E. coli* detection. These methods generally involve probe immobilization onto a transducer; the bio-recognition event is converted into electrical signal by the transducer. The immobilized probe can be an antigen,[11] DNA[12] or enzyme.[13] Label-free electrochemical detection of *E. coli* was reported on various transducers such as a self-assembled monolayer,[14] polyaniline nanotubes,[15] indium tin oxide,[16] and an interdigitated array microelectrode.[17] In this work, graphene nanosheets were employed as transducers for *E. coli* detection due to their remarkable electron mobility.

The Nobel Prize-winning isolation and characterization of graphene in 2004 added a new dimension to many applications such as electronics,[18] photonics,[19] energy[20] and sensors.[21] Graphene is a two-dimensional array of sp^2-hybridized carbon atoms in a honeycomb lattice with exceptional mechanical, thermal and electronic properties.[22,23] Though it is equipped with fascinating electronic properties, graphene nanosheets are hydrophobic in nature, hindering their application in aqueous solution. Thus, surface functionalization is needed to tailor graphene for various applications. In order to preserve high electron mobility in graphene networks, surface functionalization is performed by non-covalent π–π stacking of pyrene derivatives. Xu *et al.* first reported the functionalization of graphene by 1-pyrenebutyrate in order to manipulate graphene solubility in aqueous solution.[24] Since then, similar functionalization approaches have been frequently employed to bind various molecules onto graphene surfaces.[25–27] The functionalization of graphene by 1-pyrenebutanoic acid succinimidyl ester for glucose oxidase immobilization was reported by Huang and co-workers.[28] Other types of pyrene derivatives, such as perylene tetracarboxylic acid, tetrakis(1-methyl-4-pyridinio)porphyrin, *etc.*, have also been employed.[29–31] Herein, we report the surface functionalization of graphene by 1-pyrenebutyric acid (PyBA) followed by *E. coli* DNA immobilization through carbodiimide linkage. The hybridization between probe DNA and complementary DNA imparted charge transfer resistance to the graphene surface, which was monitored by electrochemical impedance spectroscopy (scheme 1).

[a]*Faculty of Industrial Sciences & Technology, Universiti Malaysia Pahang, 26300 Gambang, Kuantan, Pahang, Malaysia. E-mail: ckfeng@ump.edu.my; Fax: +60 95492766; Tel: +60 95492403*

[b]*Southeast Asia Disaster Prevention Research Initiative (SEADPRI-UKM), LESTARI, Universiti Kebangsaan Malaysia, 43600 UKM Bangi, Selangor, Malaysia*

† Electronic supplementary information (ESI) available. See DOI: 10.1039/c4ay01836b

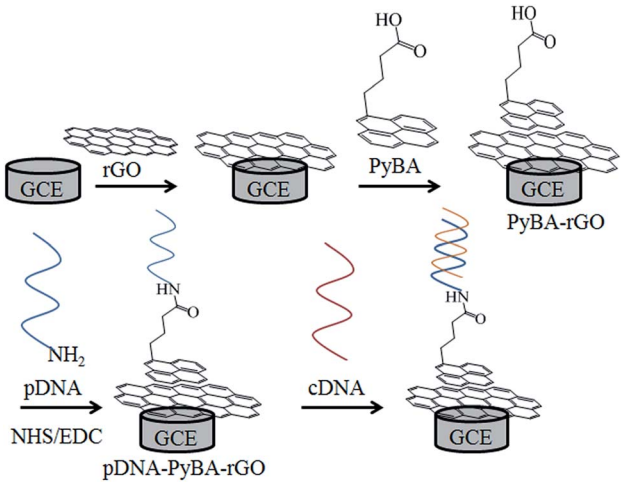

Scheme 1 Schematic representation of rGO functionalization with PyBA, pDNA immobilization and hybridization.

Experimental

Preparation of DNA materials

A complete DNA sequence (2805 bp) of Intimin (eaeA) gene of *Escherichia coli* O157:H7 strain GZ-021210 (GenBank Accession no.: EF079676.1) was retrieved from the NCBI GenBank database. A 30-oligonucleotide target of single-stranded DNA (ssDNA) as probe DNA (pDNA) was designed at a base location of 1720–1749 of the gene with an additional amine functional group at the 5′ end of the nucleotide sequence. A reverse-complement of the pDNA sequence was designed as target DNA (cDNA), while the same sequence as the probe DNA was designed for its non-complementary DNA (ncDNA). All the pDNA, cDNA and ncDNA summarized in Table 1 were synthesized by Bioneer, Korea.

Graphene synthesis

Graphite powder (Merck) was pre-oxidized in order to prevent incomplete oxidation. Briefly, graphite powder (20 g) was added into a solution of H_2SO_4 (30 mL), $K_2S_2O_8$ (10 g) and P_2O_5 (10 g) and heated at 80 °C for 6 h. The mixture was then diluted with distilled water, filtered and washed until the filtrate became pH neutral. The pre-oxidized graphite powder was dried overnight at room temperature before oxidation by Hummers' method.[32] The pre-oxidized graphite powder (20 g) was added into H_2SO_4 (460 mL), followed by the addition of $KMnO_4$ (60 g, Merck). The addition of $KMnO_4$ was performed slowly with stirring and cooling to maintain the temperature of the mixture at 20 °C. The mixture was then stirred at 35 °C for 2 h before distilled water (1 L) was added. The stirring was continued for 15 min, and additional distilled water (3 L) and 30% H_2O_2 (50 mL) were added into the mixture. The mixture was filtered, washed with 1 : 10 HCl and dried overnight (60 °C) in vacuum to obtain the dry graphite oxide. The exfoliation of graphite oxide was conducted by sonication (200 W) of the graphite oxide dispersion (2 mg mL^{-1}) for 30 min. It was later centrifuged at 10 000×*g* for 10 min to remove the unexfoliated graphite oxide. Graphene oxide dispersion was obtained as a homogeneous yellow brown supernatant. The graphene oxide was reduced by adding hydrazine monohydrate (0.25 mL) into the graphene oxide dispersion. The mixture was refluxed at 95 °C for 24 h. Dried reduced graphene oxide (rGO) was obtained by vacuum filtration, washing with distilled water and drying overnight (60 °C) in vacuum.

Table 1 List of DNA (oligonucleotide) sequences

Sequences	From 5′ to 3′
ssDNA (pDNA)	NH_2-AAC GCC GAT ACC ATT ACT TAT ACC GCG ACG
Target DNA (cDNA)	CGT CGC GGT ATA AGT AAT GGT ATC GGC GTT
Non-complementary DNA (ncDNA)	AAC GCC GAT ACC ATT ACT TAT ACC GCG ACG

Functionalization and hybridization

A glassy carbon electrode (CH Instruments) was polished with alumina powder and sequentially sonicated in ultrapure water and anhydrous ethanol. The graphene electrode was made by drop-casting an rGO suspension (2 mg mL^{-1} in ethanol) onto the polished glassy carbon electrode. The graphene electrode was dried under N_2 flow. Graphene functionalization was performed by dropping 1-pyrenebutyric acid (10 mM) onto the graphene electrode and allowing it to dry at room temperature for 30 min. This electrode was termed the PyBA–rGO electrode. The loosely attached PyBA was removed by rinsing the PyBA–rGO electrode with ultrapure water. The immobilization of pDNA onto PyBA–rGO was carried out using carbodiimide linkage chemistry. The carboxyl group of PyBA was activated by immersing the PyBA–rGO electrode in a phosphate-buffered solution containing *N*-(3-dimethylaminopropyl)-*N*′-ethyl-carbodiimide hydrochloride (5 mM) and *N*-hydroxysuccinimide (8 mM) for 30 min. To immobilize the pDNA of *E. coli*, pDNA (1.0×10^{-10} M) was incubated for 30 min. The unbound pDNA was removed by rinsing with 0.2% sodium dodecyl sulphate and ultrapure water. Hybridization was conducted by incubating the pDNA–PyBA–rGO electrode with hybridization solution containing different concentrations of target DNA for 30 min. Subsequently, the electrode was rinsed three times with ultrapure water.

Characterization

UV-vis absorption spectra were recorded using a GENESYS 10 UV spectrophotometer (Thermo Scientific). The surface morphology of reduced graphene oxide was studied by field emission scanning electron microscopy (FESEM; JEOL JSM-7800F). The Raman spectrum of reduced graphene oxide was examined by using a Renishaw (In-Via) Raman microscope with a 532 nm laser as the excitation source.

Electrochemical measurements

A three-electrode system was constructed for electrochemical measurements with a modified electrode as working electrode, platinum wire (CH Instruments) as counter electrode, and Ag/AgCl (CH Instruments) as reference electrode. A PARSTAT2273 (Princeton Applied Research) potentiostat was used to perform the electrochemical measurements. All measurements were carried out at room temperature in an enclosed and grounded Faraday cage. Cyclic voltammetry (CV) tests were performed in the potential range of 0.2 V to 0.6 V *versus* Ag/AgCl. Electrochemical impedance spectroscopy (EIS) data were collected from 500 kHz to 10 mHz using an open circuit potential with an a.c. amplitude of 10 mV. All electrochemical measurements were performed in 0.1 M phosphate-buffered saline with $K_3[Fe(CN)_6]/K_4[Fe(CN)_6]$ (5.0 mM).

Results and discussion

Characterization of reduced graphene oxide

UV-vis spectroscopy allows the visualization of the restoration of electronic conjugation in reduced graphene oxide. The shifting of the UV absorption band from *ca.* 230 nm to *ca.* 270 nm signifies the complete reduction process for graphene oxide.[33] As shown in Fig. 1, the initial position of the absorption peak of graphene oxide of 230 nm was shifted to 270 nm after the reduction process. This confirms that the graphene oxide was fully reduced.

Fig. 2 shows the FESEM image of reduced graphene oxide. Curvy and wrinkled sheets, attributed to the exfoliation treatment during synthesis, are clearly observed. This expanded morphology is essential in the immobilization process as it maximizes the surface area available for DNA immobilization.

Raman spectroscopy is a powerful non-destructive tool to characterize the electronic structures of carbonaceous materials. The Raman spectrum of reduced graphene oxide is shown in Fig. 3. There are two main features in the Raman spectrum of graphene material: the G band (*ca.* 1580 cm^{-1}) and the D band (*ca.* 1345 cm^{-1}). The G band is assigned to the first order scattering of the E_{2g} phonons of sp^2 carbon atoms, while the D band is the breathing mode of κ-point phonons with A_{1g} symmetry.[34] The Raman spectrum of reduced graphene oxide shows that there was a substantial increase in the D band intensity and a shifting of the G band to 1591 cm^{-1}. The results suggest the formation of in-plane sp^2 graphene domains with smaller sizes and higher defect sites.

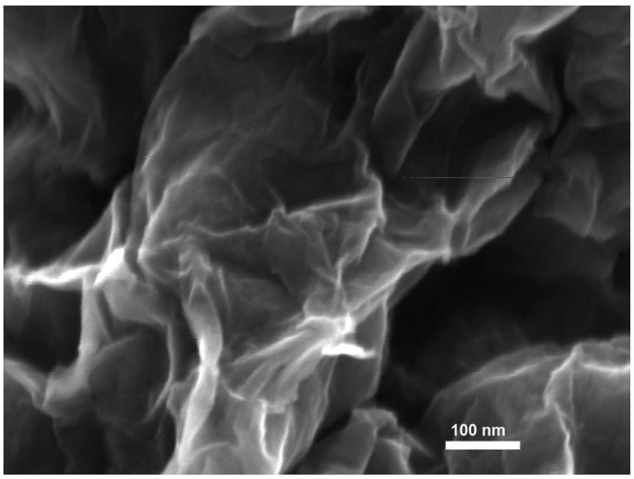

Fig. 2 FESEM image of reduced graphene oxide.

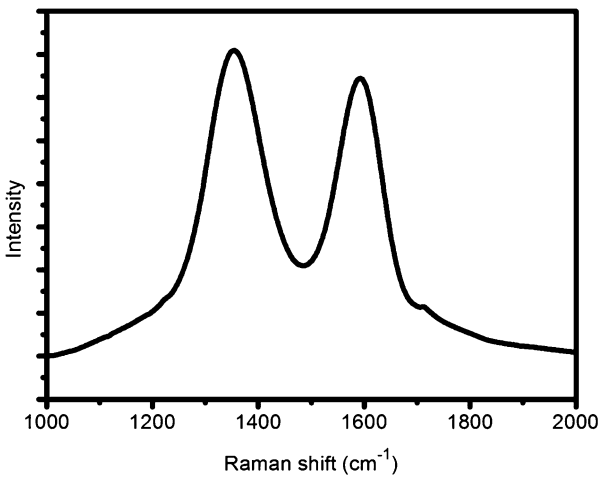

Fig. 3 Raman spectrum of reduced graphene oxide.

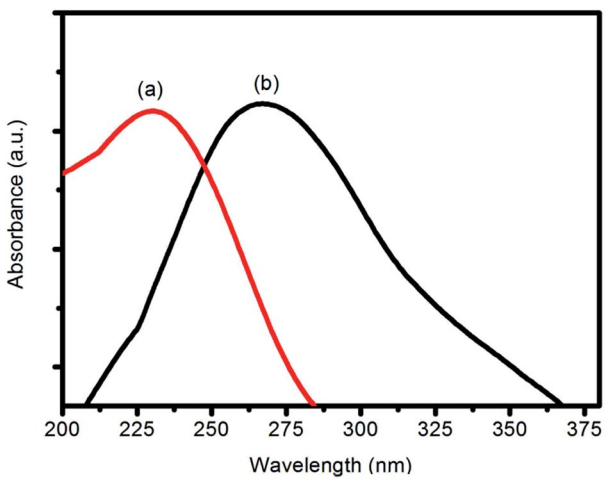

Fig. 1 UV-vis spectra of (a) graphene oxide and (b) reduced graphene oxide.

Electrochemical characterization of the PyBA–rGO electrode

The functionalization of PyBA was monitored by CV and EIS in the electrolyte system containing $[Fe(CN)_6]^{3-/4-}$, as shown in Fig. 4.

Before rGO deposition, a pair of well-defined redox peaks could be observed on the glassy carbon electrode with a peak separation (ΔE_p) of 0.16 V. After rGO deposition, the increment in peak current could be observed, accompanied by larger ΔE_p (0.22 V). The higher peak current for the rGO-modified electrode can be attributed to the expanded morphology of rGO, which

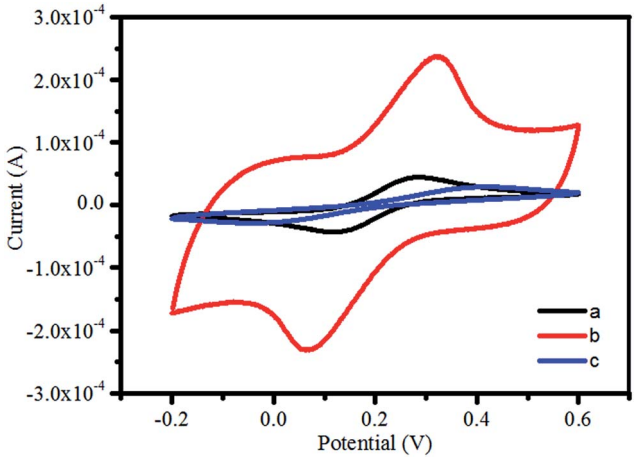

Fig. 4 Cyclic voltammogram recorded at (a) glassy carbon electrode (b) rGO-modified electrode and (c) PyBA–rGO modified electrode in the presence of 5.0 mM $[Fe(CN)_6]^{3-/4-}$.

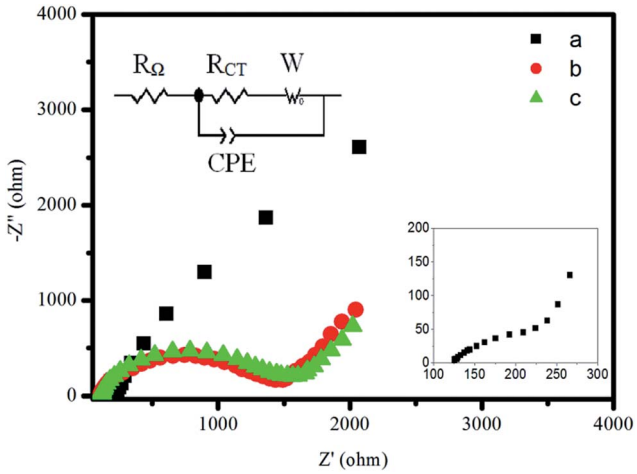

Fig. 5 Nyquist plots for (a) rGO-modified electrode, (b) PyBA–rGO modified electrode and (c) pDNA–PyBA–rGO modified electrode. Insets show the equivalent circuit for the modified electrode (top) and the Nyquist plot for (a) at a high frequency region (bottom).

provides a higher surface area (152 $m^2\ g^{-1}$, ESI†) for the electron transfer reaction. On the other hand, the larger ΔE_p is attributed to the contact resistance between rGO and the glassy carbon electrode.[35] In addition, a huge capacitance was observed on the rGO-modified electrode as graphene nanosheets were proven to possess large electrical double layer capacitances.[36] After functionalization with PyBA, the ΔE_p increased to 0.45 V, with a lower peak current than the rGO-modified electrode. This is mainly due to the electrostatic repulsion between $[Fe(CN)_6]^{3-/4-}$ and negatively charged PyBA. The CV results suggest that the rGO-modified electrode was successfully functionalized with PyBA.

The electrochemical sensing of *E. coli* O157:H7 DNA was monitored by EIS, which is a powerful tool to analyse the complex resistance of a system and is very sensitive to changes on the electrode surface. In the field of biosensing, EIS is particularly suitable to detect the bio-recognition event that occurs at the electrode–electrolyte interface, such as DNA hybridization[37,38] and antigen–antibody binding.[39,40]

Fig. 5 shows the Nyquist plots for modified electrodes. The impedances of the modified electrodes can be represented by the equivalent circuit, as shown in Fig. 5 inset (top), where R_Ω is the bulk solution resistance, R_{CT} is the charge transfer resistance, CPE is the constant phase element and W is the Warburg impedance resulting from diffusion. Briefly, the R_{CT} of the electrode can be estimated from the interception of the semicircle plot with the x axis. The larger semicircle represents the larger R_{CT}. In this work, R_{CT} was monitored as it is sensitive to surface modification. The surface functionalization in this work occurred through π–π interactions in order to preserve the electronic conductivity of rGO. However, the functionalization induced a higher R_{CT} on the PyBA–rGO-modified electrode, as shown in Fig. 5b. As suggested by the CV results, the electrostatic repulsion between $[Fe(CN)_6]^{3-/4-}$ and the negatively charged PyBA imposed a higher R_{CT} on the modified electrode. The immobilization of pDNA on the PyBA–rGO modified electrode was performed by carbodiimide covalent linkage to prevent the detachment of DNA from the electrode surface. After immobilization, the R_{CT} of the pDNA–PyBA–rGO electrode also increased (Fig. 5c), mainly due to the electrostatic repulsion of the negatively charged DNA backbone as well as the non-conducting nature of the DNA backbone. The calculated R_{CT} values of the modified electrodes are summarized in Table 2.

DNA biosensing

In this work, the *E. coli* O157:H7 DNA was detected by monitoring the R_{CT} of the pDNA–PyBA–rGO-modified electrode during the DNA hybridization process.

Fig. 6 shows the Nyquist plots of the pDNA–PyBA–rGO-modified electrode after incubation with cDNA at different concentrations. Upon hybridization, the more negatively charged phosphate backbones of DNA could be found on the electrode–electrolyte interface. These created more repulsive forces with the redox species $[Fe(CN)_6]^{3-/4-}$, leading to a higher R_{CT} at higher cDNA concentrations. It can be seen that rGO was very sensitive to the surface changes; the low cDNA concentration of 1.0×10^{-14} M induced a *ca.* 30% increase in R_{CT} compared to the blank solution.

Fig. 7 plots R_{CT} as a function of cDNA concentration. A linear response for *E. coli* DNA detection is observed in the cDNA concentration range from 1.0×10^{-14} M to 1.0×10^{-10} M; the regression equation was $\Delta R_{CT} = 2238.6 \log C + 34\,787$, with a regression coefficient (R^2) of 0.9938. The detection limit

Table 2 R_{CT} of the rGO electrode, PyBA–rGO-modified electrode and pDNA–PyBA–rGO-modified electrode

Electrode	R_{CT} (ohm)
rGO	125
PyBA–rGO	1227
pDNA–PyBA–rGO	1343

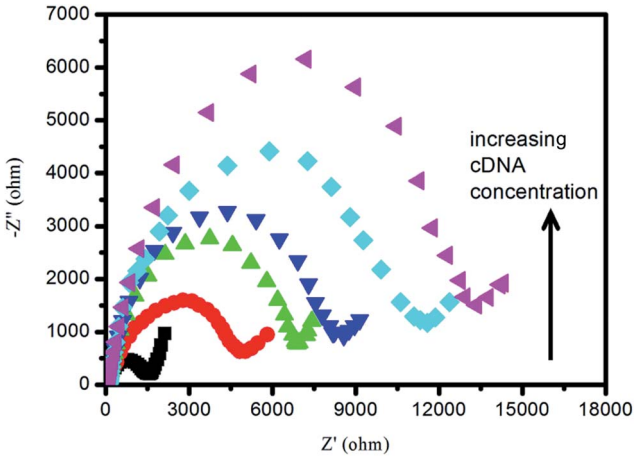

Fig. 6 Nyquist plots of the pDNA–PyBA–rGO modified electrode after cDNA hybridization at increasing cDNA concentrations of 0, 1.0×10^{-14}, 1.0×10^{-13}, 1.0×10^{-12}, 1.0×10^{-11} and 1.0×10^{-10} M.

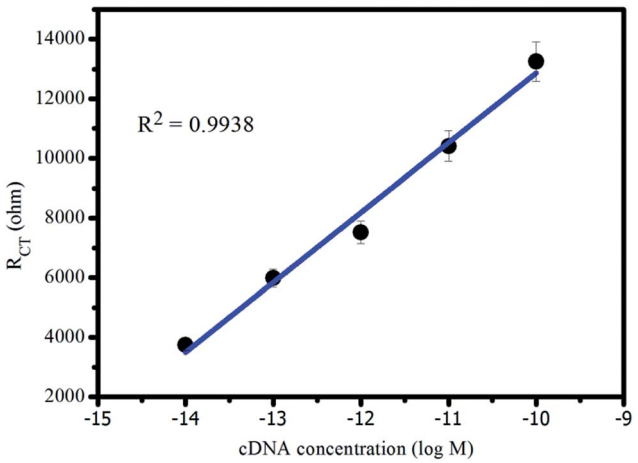

Fig. 7 R_{CT} *vs.* cDNA concentration (log scale).

obtained as three times the standard deviation of the blank was calculated to be 0.7×10^{-15} M. In order to gain a better understanding of biosensor performance in terms of cell number, the DNA concentration was converted into number of cells; the result of this calculation is shown in ESI.† The linear response range of the modified electrode was calculated to be 6.02×10^5 to 6.02×10^9 cells mL^{-1}, with a detection limit of 4.22×10^5 cells mL^{-1}. The detection limit of the modified electrode is comparable with other methods such as immunomagnetic separation/flow injection analysis/mediated amperometric detection ($\sim 10^5$ cells mL^{-1})[41] and optical immunoassay using tetramethylbenzidine as a substrate (10^5 cells mL^{-1}).[42]

DNA biosensor robustness, selectivity and reproducibility

The robustness of a biosensor is very important to ensure the continuous usage of the biosensor without the need for frequent replacement. The robustness of the pDNA–PyBA–rGO-modified electrode was tested by a continuous hybridization–dehybridization process. The dehybridization process was performed in NaOH solution (10 mM).

Fig. 8 shows the Nyquist plots of the pDNA–PyBA–rGO-modified electrode before and after four cycles of the hybridization–dehybridization process. The robustness of the biosensor is demonstrated by the restoration of R_{CT} after four hybridization–dehybridization cycles. This result is attributed to the strong π–π interaction between rGO and PyBA, as well as the sturdy covalent linkage between PyBA and pDNA. The strong interaction within the modified electrode allowed it to be recycled for usage even after multiple washing cycles during the dehybridization process.

The selectivity of a biosensor is crucial for accurate bioanalyte detection. The selectivity of the pDNA–PyBA–rGO-modified electrode towards *E. coli* O157:H7 DNA was tested by incubating the modified electrode with mismatch DNA sequences, as well as with the ncDNA; the results are shown in Fig. 9.

Testing with ncDNA revealed a drastic decrease in the R_{CT} as compared to the results obtained with cDNA. However, the ncDNA testing is not sufficient to demonstrate the selectivity of the modified electrode, and further tests were thus conducted with mismatch DNA sequences. All mismatch DNA sequences decreased the R_{CT}. It is worth noting that even the single-base mismatch generated a *ca.* 14% decrease in R_{CT} as compared to the cDNA. The results suggest that the pDNA–PyBA–rGO electrode is highly selective as it could differentiate a DNA mismatch, even if only of a single base pair. The high selectivity of the modified electrode can be attributed to the good electron mobility of rGO as a transducer, making it sensitive to any changes in surface conductivity.

The reproducibility of the DNA biosensor was tested on four different pDNA–PyBA–rGO-modified electrodes. The pDNA–PyBA–rGO-modified electrodes demonstrated good reproducibility (Table 3); all modified electrodes showed relative standard deviations (RSD) lower than 5%.

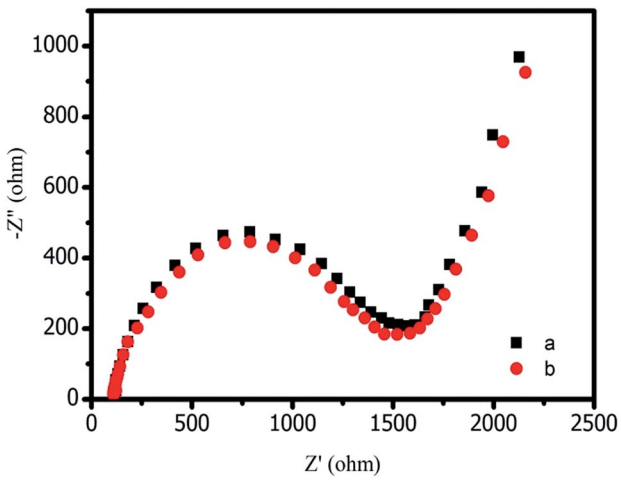

Fig. 8 Nyquist plots of pDNA–PyBA–rGO-modified electrode (a) before and (b) after 4 cycles of the hybridization–dehybridization process with cDNA (1.0×10^{-10} M).

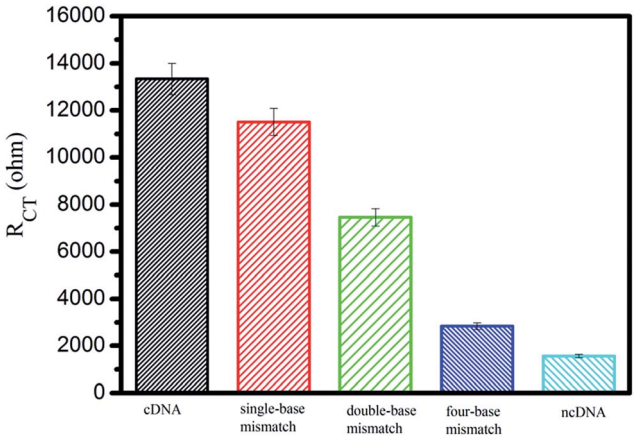

Fig. 9 R_{CT} of pDNA–PyBA–rGO-modified electrode with mismatch DNA and ncDNA. All DNA strains were tested at 1.0×10^{-10} M.

Table 3 R_{CT} of different pDNA–PyBA–rGO-modified electrodes

	R_{CT} (ohm)	
Modified electrode	Before hybridization	After hybridization
pDNA–PyBA–rGO 1	1343	13 133
pDNA–PyBA–rGO 2	1332	13 245
pDNA–PyBA–rGO 3	1366	13 046
pDNA–PyBA–rGO 4	1323	13 160
RSD	1.34%	0.62%

Conclusion

In summary, a simple *E. coli* O157:H7 DNA strain GZ-021210 biosensor was constructed by graphene surface functionalization followed by pDNA immobilization. Electrochemical studies demonstrated the successful pDNA immobilization, and the hybridization of cDNA was monitored by EIS. The modified electrode showed a linear response range from 1.0×10^{-14} M to 1.0×10^{-10} M with a detection limit of 0.7×10^{-15} M. In addition, the modified electrode showed high robustness, selectivity and reproducibility.

Acknowledgements

KF Chong and co-workers would like to acknowledge the funding from the Ministry of Education Malaysia in the form of MTUN-COE grant RDU121217 and ERGS RDU120604.

References

1 A. D. Chowdhury, A. De, C. R. Chaudhuri, K. Bandyopadhyay and P. Sen, *Sens. Actuators, B*, 2012, **171**, 916–923.
2 W. Keene, E. Sazie, D. Rice, D. Hancock, V. Balan, T. Zhao and M. Doyle, *JAMA, J. Am. Med. Assoc.*, 1997, **227**, 1229–1231.
3 D. Ivnitski, I. Abdel-Hamid, P. Atanasov and E. Wilkins, *Biosens. Bioelectron.*, 1999, **14**, 599–624.
4 *E. coli* rapid response in a crisis. In Wikipedia. Retrieved October 2, 2012,from http://en.wikipedia.org/wiki/European Food Safety Authority.
5 H. Lei, Y. Zhang, X. Li and B. Li, *Lab Chip*, 2011, **11**, 2241–2246.
6 H. Xin, C. Cheng and B. Li, *Nanoscale*, 2013, **5**, 6720–6724.
7 R. L. Schelonka, M. K. Chai, B. A. Yoder, D. Hensley, R. M. Brockett and D. P. Ascher, *J. Pediatr.*, 1996, **129**, 275–278.
8 J. Lerchner, A. Schulz, T. Poeschel, A. Wolf, T. Hartmann, F. Mertens and E. Boschke, *Eng. Life Sci.*, 2012, **12**, 615–620.
9 I. H. Park, Y. H. Heo, P. Kim and K. S. Nahm, *RSC Adv.*, 2013, **3**, 16665–16671.
10 Y. Hu, F. Li, X. Bai, D. Li, S. Hua, K. Wang and L. Niu, *Chem. Commun.*, 2011, **47**, 1743–1745.
11 J. J. Gooding, C. Wasiowych, D. Barnett, D. B. Hibbert, J. N. Barisci and G. G. Wallace, *Biosens. Bioelectron.*, 2004, **20**, 260–268.
12 S. Niu, M. Zhao, L. Hu and S. Zhang, *Sens. Actuators, B*, 2008, **135**, 200–205.
13 P. Bertocchi, D. Compagnone and G. Palleschi, *Biosens. Bioelectron.*, 1996, **11**, 1–10.
14 E. P. Randviir and C. E. Banks, *Anal. Methods*, 2013, **5**, 1098–1115.
15 H. Chang, Y. Yuan, N. Shi and Y. Guan, *Anal. Chem.*, 2007, **79**, 5111–5115.
16 C. Ruan, L. Yang and Y. Li, *Anal. Chem.*, 2002, **74**, 4814–4820.
17 P. Zhu, D. R. Shelton, S. Li, D. L. Adams, J. S. Karns, P. Amstutz and C. M. Tang, *Biosens. Bioelectron.*, 2011, **30**, 337–341.
18 H. Zhu, P. Huang, L. Jing, T. Zuo, Y. Zhao and X. Gao, *J. Mater. Chem.*, 2012, **22**, 2063–2068.
19 X. Gan, R. J. Shiue, Y. Gao, K. F. Mak, X. Yao, L. Li, A. Szep, D. Walker, J. Hone, T. F. Heinz and D. Englund, *Nano Lett.*, 2013, **13**, 691–696.
20 A. I. Aria, A. W. Gani and M. Gharib, *Appl. Surf. Sci.*, 2014, **293**, 1–11.
21 T. T. Tung, M. Castro, T. Y. Kim, K. S. Suh and J. F. Feller, *J. Mater. Chem.*, 2012, **22**, 21754–21766.
22 X. Zhou, T. Wu, B. Hu, G. Yang and B. Han, *Chem. Commun.*, 2010, **46**, 3663–3665.
23 S. Stankovich, D. A. Dikin, G. H. B. Dommett, K. M. Kohlhaas, E. J. Zimney, E. A. Stach, R. D. Piner, S. T. Nguyen and R. S. Ruoff, *Nature*, 2006, **442**, 282–286.
24 Y. Xu, H. Bai, G. Lu, C. Li and G. Shi, *J. Am. Chem. Soc.*, 2008, **130**, 5856–5857.
25 Z. Wang, P. Huang, A. Bhirde, A. Jin, Y. Ma, G. Niu, N. Neamati and X. Chen, *Chem. Commun.*, 2012, **48**, 9768–9770.
26 F. Liu, K. S. Choi, T. J. Park, S. Y. Lee and T. S. Seo, *BioChip J.*, 2011, **5**, 123–128.
27 K. P. Loh, Q. Bao, P. K. Ang and J. Yang, *J. Mater. Chem.*, 2010, **20**, 2277–2289.
28 Y. Huang, X. Dong, Y. Shi, C. M. Li, L. J. Li and P. Chen, *Nanoscale*, 2010, **2**, 1485–1488.

29 Y. Hu, F. Li, X. Bai, D. Li, S. Hua, K. Wang and L. Niu, *Chem. Commun.*, 2011, **47**, 1743–1745.
30 Y. Hu, F. Li, D. Han, T. Wu, Q. Zhang, L. Niu and Y. Bao, *Anal. Chim. Acta*, 2012, **753**, 82–89.
31 Y. Xu, L. Zhao, H. Bai, W. Hong, C. Li and G. Shi, *J. Am. Chem. Soc.*, 2009, **131**, 13490–13497.
32 W. S. Hummers and R. E. Offeman, *J. Am. Chem. Soc.*, 1958, **80**, 1339.
33 D. Li, M. B. Müller, S. Gilje, R. B. Kaner and G. G. Wallace, *Nat. Nanotechnol.*, 2008, **3**, 101–105.
34 D. A. Brownson, S. A. Varey, F. Hussain, S. J. Haigh and C. E. Banks, *Nanoscale*, 2014, **6**, 1607–1621.
35 R. Ramesham, *Sens. Actuators, B*, 1998, **50**, 131–139.
36 M. D. Stoller, S. Park, Z. Yanwu, J. An and R. S. Ruoff, *Nano Lett.*, 2008, **8**, 3498–3502.
37 K. Kerman, Y. Morita, Y. Takamura and E. Tamiya, *Anal. Bioanal. Chem.*, 2005, **381**, 1114–1121.
38 L. Wang, Q. Liu, Z. Hu, Y. Zhang, C. Wu, M. Yang and P. Wang, *Talanta*, 2009, **78**, 647–652.
39 W. Dou, W. Tang and G. Zhao, *Electrochim. Acta*, 2013, **97**, 79–85.
40 Y. Teng, X. Zhang, Y. Fu, H. Liu, Z. Wang, L. Jin and W. Zhang, *Biosens. Bioelectron.*, 2011, **26**, 4661–4666.
41 F. G. Perez, M. Mascini, I. E. Tothill and A. P. F. Turner, *Anal. Chem.*, 1998, **70**, 2380–2386.
42 K. H. Shim, M. Kang, M. G. Kim, B. H. Chung and S. S. A. An, *J. Toxicol. Environ. Health Sci.*, 2011, **3**, 80–85.